Design of Cellular Porous Biomaterials for Wall Shear Stress Criterion

Yuhang Chen, Shiwei Zhou, Joseph Cadman, Qing Li

School of Aerospace, Mechanical and Mechatronic Engineering, University of Sydney, NSW 2006, Australia; telephone: 61-2-9351-8607; fax: 61-2-9351-7060; e-mail: qing.li@sydney.edu.au

ABSTRACT: The microfluidic environment provided by implanted prostheses has a decisive influence on the viability, proliferation and differentiation of cells. In bone tissue engineering, for instance, experiments have confirmed that a certain level of wall shear stress (WSS) is more advantageous to osteoblastic differentiation. This paper proposes a level-set-based topology optimization method to regulate fluidic WSS distribution for design of cellular biomaterials. The topological boundary of fluid phase is represented by a level-set model embedded in a higher-dimensional scalar function. WSS is determined by the computational fluid dynamics analysis in the scale of cellular base cells. To achieve a uniform WSS distribution at the solid–fluid interface, the difference between local and target WSS is taken as the design criterion, which determines the speed of the boundary evolution in the level-set model. The examples demonstrate the effectiveness of the presented method and exhibit a considerable potential in the design optimization and fabrication of new prosthetic cellular materials for bioengineering applications.

Biotechnol. Bioeng. 2010;107: 737–746.

© 2010 Wiley Periodicals, Inc.

KEYWORDS: cellular material; level-set method; wall shear stress; solid free-form fabrication; tissue engineering; biofluid

Introduction

Materials with cellular microstructures are commonly observed in biological systems (Gibson, 2005). Such porous structures provide a sophisticated network to transport biofluids inside natural biomaterials (Katayama et al., 1999). Recently, cellular materials have been widely used in various biomedical areas. Tissue engineering, as one such cutting-edge technology, has aimed to replace damaged tissue/organ or generate neo-tissue for restoring biological functions. In this context, artificial porous scaffolds are considered critical

to create a desirable biomechanical condition for cell proliferation and differentiation. One common approach to scaffold design has been to mimic the native extracellular matrix, thereby imitating a cell-friendly environment. In essence, the regeneration of neo-tissue within desirable tissue-scaffold constructs requires proper biocompatibity to enable sufficient cell migration, nutrition delivery, metabolite removal, unhindered neo-vascularization, and other biomechanical conditions (Rose and Oreffo, 2002). With the rapid development of various biodegradable materials and micro/nano-fabrication technologies, porous cellular biomaterials have been found particularly promising for their superior capability of providing a desired biomimetic environment (Hollister, 2005, 2009).

In general, biodegradable cellular materials used in therapeutic tissue regeneration should possess desired multifunctionality, including (1) adequate biocompatibility to ensure a proper biochemical environment for cell proliferation and differentiation, (2) sufficient porosity for mass transfer and vascularization, (3) controllable biodegradable rate of the matrix materials, and (4) adaptive mechanical properties that include not only the similar load-bearing capacities to surrounding tissues, but the cell-favorable microfluidic properties in terms of flow velocity and wall shear stress (WSS). Of these multifunctional properties, the studies on microfluidic WSS have been rather limited, though it plays a critical role in tissue regeneration (Hillsley and Frangos, 1994).

The effects of fluidic shear stress on the success of tissue engineering have been recognized in different ways. From a cell perspective, it is known that flow-mediated shear stress is a key modulator to regulate cell function (Gemmiti and Guldberg, 2009; McAllister and Frangos, 1999). Sakai et al. (1998) showed that a certain physiological level of fluid shear stress can increase mRNA expression in human osteoblast-like cell by approximately threefold, thus better promoting bone formation. A constitutive nitric oxide (NO) isoform was observed in osteoblasts that was significantly affected by fluid flow, suggesting that the flow plays a

primary role in determining bone maintenance and remodeling (Johnson et al., 1996). The comparison of production rates of NO and prostaglandin E2 (PGE2) from bone cells subject to unidirectional linear strains and fluid flow further showed that the mechanical loading can be sensed by osteoblasts through flow-mediated WSS rather than pure mechanical strain (Smalt et al., 1997).

From a scaffold perspective, the tissue growth has been explored under different flow conditions; and it is found that the osteogenesis can be modulated by the local flow environment (Meinel et al., 2004). It has been proven that cell detachment is enhanced by increasing the physiological shear stress for the endothelium lining of vessels (Davies, 1995) and a linear relationship between cell detachment and mechanical shear stress was established (Powers et al., 1997). Based on these findings, Provin et al. (2008) suggested that a certain range of flow rate and shear stress could be crucial for both cell attachment and tissue regeneration. Indeed, the biological advantages of a *uniform* WSS distribution in bioreactors and scaffolds have been confirmed (Gao et al., 1997). A uniform hydrodynamic environment corresponded well with a more uniform tissue growth (Cioffi et al., 2006; Gutierrez and Crumpler, 2008; Saini and Wick, 2001; Williams et al., 2002). Thus, in order to obtain a more desirable tissue ingrowth within scaffold, a homogeneous WSS distribution appears important.

Design and fabrication of sophisticated biomaterial configuration for promoting tissue growth signify an important research topic (Lacroix et al., 2009). As a critical issue, the understanding of the in-scaffold microfluidic characteristics is essential. In this respect, majority of existing studies has been experimentally oriented. Recently, mathematical modeling has drawn increasing attention, aiming to gain a more comprehensive understanding of the fluidic fields and shorten a laborious trial-and-error experimental process (Hutmacher and Singh, 2008). For example, the flow conditions were simulated within cylindrical scaffolds, which identified the significant needs for optimizing the fluidic shear stress in biomaterial microstructures (Porter et al., 2005). Furthermore, the shear stress distributions in different pore geometries were quantified in the computational fluid dynamic (CFD) model for 3D scaffolds, showing that both pore size and porosity could influence in-scaffold fluidic shear stress, thus affecting the tissue ingrowth (Boschetti et al., 2006). More recently, various numerical studies were carried out to analyze WSS and other mechanical stimuli in a 3D porous scaffold structure (Cioffi et al., 2006), face-centered cubic-based structure (Lesman et al., 2010) and irregular 3D cellular scaffold under direct perfusion cultures (Maes et al., 2009), respectively. The interplays between WSS and tissue growth in cellular cell-scaffold constructs (Chung et al., 2007) as well as a polylactic acid–calcium phosphate glass scaffold (Milan et al., 2009) were explored. Despite these successful theoretical and experimental studies, how to design and fabricate porous cellular materials with desirable WSS levels and patterns remains rather challenging.

Topology optimization, as a powerful tool in structural design, has proven effective in seeking optimal porous configurations in a range of applications. Over the last two decades, a range of density-based algorithms (e.g., solid isotropic material with penalization—SIMP, Bendsoe and Sigmund, 2003 and evolutionary structural optimization—ESO, Steven et al., 2000), in which the relative density of each finite element is treated as a design variable and empirically related to some material properties, have drawn significant attention for their proven capabilities in tackling structural topological optimization problems. In this respect, an image-based homogenization approach to the base-cell design of scaffolds appears fairly effective, where the stiffness tensor calculated from the homogenization procedure was matched to the desired stiffness of host bone while maintaining the same porosity (Hollister et al., 2002). Furthermore, Hollister and Lin (2007) applied homogenization-based optimization approaches for design of scaffold architectures. Guest and his colleagues adopted the permeability criterion to maximize the permeable fluid capacity of a porous medium (Guest and Prevost, 2006, 2007). Recently, the permeability and diffusivity criteria were combined with the stiffness criterion of the host bone for the design of cellular materials and a series of optimal topologies that match the mechanical and fluidic properties to different bone tissues were obtained (Chen et al., 2009; Kang et al., 2010).

As a relatively new technique, the level-set method that was developed originally in image processing (Osher and Sethian, 1988) has demonstrated superior capability of tracking dynamically propagating interfaces in topology optimization, ranging from structural (Sethian and Wiegmann, 2000; Wang et al., 2003) to fluidic designs (Challis and Guest, 2009; Zhou and Li, 2008). Sethian and Wiegmann's (2000) early work showed the applicability of the level-set technique in optimizing elastic structures, where local von Mises stress was directly taken as the level-set velocity for driving the structural boundaries. In fluidic optimization, a level-set algorithm for the steady-state Navier–Stokes flow, where the solid–fluid interface was determined for maximizing permeability and minimizing energy dissipation in the periodic cellular materials, was also established (Zhou and Li, 2008). On one hand, the explorations in fluidic problems exhibited some evident advantages due to a smooth mathematical representation of fluid–solid boundaries. On the other hand, these studies aimed to optimize the fluidic structures and materials for some energy-type objectives, where design sensitivity can be derived for the level-set velocity. Unfortunately, none of the existing studies has been related to the WSS criteria despite its critical importance in determining cell function and tissue differentiation. Thus in this paper, we will develop a level-set-based procedure to seek optimal base-cell topology for the uniformity of WSS in periodic cellular biomaterials, thereby providing a new class of porous medium for such

biomedical applications as tissue scaffolds, cardiologic stents, and porous coated implants.

Materials and Methods

To develop the level-set procedure specifically for the WSS criterion in cellular microstructural materials, descriptions of the design problem, the level-set model, and the numerical algorithm are presented in this section.

Design Optimization

Biomaterials with periodic cellular microstructure are widespread in natural and synthetic constructs and generally involve two significant length-scales, one in macroscopic material level and another in microscopic base-cell level. Both experimental and mathematical analyses show that the effective (bulk) material properties can be largely affected by the microstructural configuration (Gibson, 2005; Hassani and Hinton, 1998), indicating that the microstructural design of cellular biomaterials is of crucial importance.

Mathematically, WSS can be defined as a total shear stress in 3D Cartesian coordinates as

$$\begin{aligned} \tau_{xy} &= \mu\left(\frac{\partial u}{\partial y} + \frac{\partial v}{\partial x}\right) \\ \tau_{yz} &= \mu\left(\frac{\partial v}{\partial z} + \frac{\partial w}{\partial y}\right) \\ \tau_{xz} &= \mu\left(\frac{\partial u}{\partial z} + \frac{\partial w}{\partial x}\right) \end{aligned} \tag{1}$$

where μ denotes the dynamic viscosity and u, v, w are the velocity components in the coordinate directions. The magnitude of WSS is calculated as

$$\tau_{\text{WSS}} = \left(\tau_{xy}^2 + \tau_{yz}^2 + \tau_{xz}^2\right)^{1/2} \tag{2}$$

Following this, to achieve a uniform WSS distribution at the fluid–solid interface, the design problem can be mathematically defined as

$$\begin{aligned} &\min \sum_{\Gamma_I} \left(\tau_{\text{WSS}} - \overline{\tau}_{\text{WSS}}\right)^2 \\ &s.t. \int_{\Omega_{\text{fluid}}} d\Omega \geq V_0 \end{aligned} \tag{3}$$

where $\overline{\tau}_{\text{WSS}}$ denotes the mean or a target WSS (τ_{WSS}) at fluid interface Γ_I and V_0 is the volume constraint of fluid domain.

Level-Set Method in Topology Optimization

The basic idea of the level-set method is to represent the topological boundaries implicitly by using a zero-level contour of a higher-dimensional scalar function $\Phi(\mathbf{x})$. The boundary movement is driven in terms of either sensitivity (Zhou and Li, 2008) or an optimality design criteria (Sethian

and Wiegmann, 2000). In general, $\Phi(\mathbf{x})$ can be defined as

$$\Phi(\mathbf{x}) < 0 \quad \forall x \in \Omega_{\text{mat}} \backslash \Gamma_b \tag{4}$$

$$\Phi(\mathbf{x}) > 0 \quad \forall x \in \Omega_{\text{void}} \backslash \Gamma_b \tag{5}$$

where Ω_{mat}, Ω_{void}, and Γ_b denote the solid domain, void/fluidic domain and interface, respectively. To obtain accurate results, $\Phi(\mathbf{x})$ is often initialized and maintained as a signed distance to the given boundary ($\Phi(\mathbf{x}) = 0 \quad \forall x \in \Gamma_b$) with a negative value as defined in Equation (4) and a positive value as Equation (5). $\Phi(\mathbf{x})$ satisfies the Eikonal equation (Wang et al., 2003),

$$|\nabla \Phi(\mathbf{x})| = 1 \tag{6}$$

As such, a zero-level contour describing the boundary interface can be defined as

$$\Gamma_b = \{\mathbf{x} : \mathbf{x} \in \Omega, \Phi(\mathbf{x}) = 0\} \tag{7}$$

The zero-level contour of the level-set function $\Phi(\mathbf{x})$ represents the topology to be optimized (Fig. 1b). For a given initial guess of $\Phi(\mathbf{x})$, it is important to determine how it evolves in order to optimize the objective.

Let us consider the dynamic form of Equation (7), expressed as

$$\Gamma(t) = \{\mathbf{x}(t) : \Phi(\mathbf{x}(t), t) = 0\} \tag{8}$$

By differentiating both sides with respect to time, a speed–evolution equation of $\Phi(\mathbf{x})$ is derived as

$$\frac{\partial \Phi(\mathbf{x})}{\partial t} = -\nabla \Phi(\mathbf{x}) \frac{d\mathbf{x}}{dt} \equiv -\nabla \Phi(\mathbf{x}) S(\mathbf{x}, \Phi) \tag{9}$$

where $S(\mathbf{x}, \Phi)$ can be considered as an evolution speed of the level-set function, which is a critical parameter in the level-set model and determines the propagation speed of the zero-level contour. In addition, the techniques of velocity
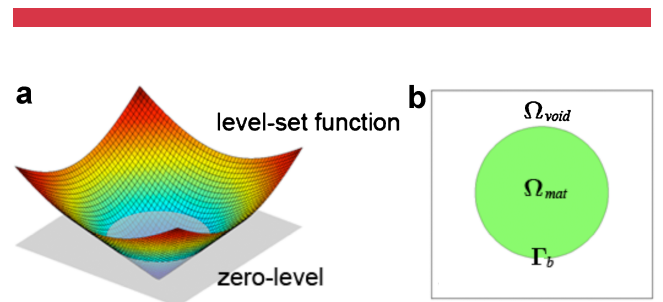
Figure 1. The level-set model. **a**: The level-set function $\Phi(\mathbf{x})$ that is initialized and maintained as a signed distance with a constant gradient (as shown in Eq. 6) to the given boundaries (the edge cut by zero-level plane). **b**: The zero-level contour that determines the topological boundary to be optimized. [Color figure can be seen in the online version of this article, available at wileyonlinelibrary.com.]

extension and reinitialization of $\Phi(\mathbf{x})$ are employed in the presented level-set procedure (Sethian and Wiegmann, 2000; Wang et al., 2003). To achieve the desired volume constraint during optimization process, a bisection algorithm is implemented in the following design examples (Zhou and Li, 2008).

Computational Fluid Dynamics (CFD) Modeling

This paper considers the design problems of 2D cross-sectional topology (or namely, quasi-3D) and full 3D base-cells (Fig. 2). Since the fluid domain is determined by the level-set model, it is convenient to extrude the 2D configuration into a 3D fluidic channel (Fig. 2a), where Γ_{in} and Γ_{out} are the inlet and outlet boundaries, respectively. The WSS at the boundary of the cross-sectional design plane is determined by the CFD analysis in a commercial software ANSYS. In the full 3D problems (Fig. 2b), the design aims to optimize the 3D fluidic porous topologies that are extracted from a 4D level-set function. In the topology optimization procedure, level-set function $\Phi(\mathbf{x})$ will be updated in terms of the deviation between local WSS and its target, which will gradually make the WSS distribution more and more uniform.

In the 2D cross-sectional channel designs, since the region of interest is axisymmetrical and located at the middle part of the flow channel, the WSS obtained from CFD analysis is independent on the flow directions. In the 3D base-cell designs, the flow direction can however affect the WSS distribution. Therefore, an additional CFD analysis with the flow from an opposite direction is required. The data gathered from both the analyses will be used for the design optimization to accommodate multi-directional flows.

Design Criterion: Uniformity of Wall Shear Stress

As abovementioned, the propagation velocity $S(\mathbf{x},\Phi)$ plays a critical role in optimizing the interfacial configuration. For the problem defined in Equation (3), a WSS-based velocity $S(\mathbf{x},\Phi)$ should be defined. In literature, the von Mises stress criterion was directly adopted to calculate the level-set velocity, aiming to achieve a uniform von Mises stress distribution in the solid structures (Sethian and Wiegmann, 2000). Specifically, the scaled velocity is considered as a function of the von Mises stress, depending on the deviation between local stress and a so-called non-shear region. Following this success, we adopt the WSS deviation to determine the propagation velocity of level-set model. If the local τ_{WSS} at a point is higher than the desired value, for example, mean $\overline{\tau}_{WSS}$, the corresponding velocity will be defined as the positive squared difference between them, moving the interface outwards from the fluid domain. In contrast, if the local τ_{WSS} at a point is lower than target $\overline{\tau}_{WSS}$, the velocity will be defined as the negative squared difference, moving the interface inwards to the fluid domain.
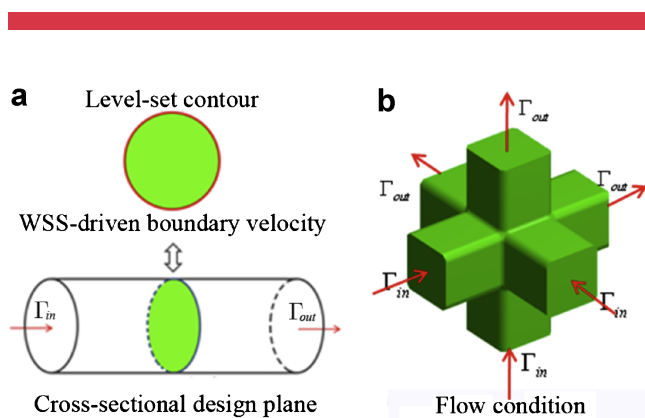
Parameter Settings for Numerical Simulation

In tissue engineering, it has been shown *in vitro* that a certain level of fluid flow can stimulate cells to respond more positively (Klein-Nulend et al., 2005). To better simulate the in-scaffold microfluid, the dimension of design domain and fluidic properties are set in line with the experimental parameters. For synthetic scaffolds, the diameter of spherical pores usually stays within 50–200 µm, depending on the function and property of the host tissue (Hollister, 2009). In this paper, the dimension of the design domain is set as 200 µm, subject to the predefined volume fraction (or porosity) constraint. Although topology optimization is independent of the absolute size, fluidic properties used in numerical computation are size-dependent and must be chosen properly to simulate the real flow conditions in porous biomaterials. In this study, the fluid is modeled as an incompressible, homogeneous, Newtonian fluid with a density of $1{,}000 \, \mathrm{kg \, m^{-3}}$ and viscosity of $8.2 \times 10^{-4} \, \mathrm{kg \, m^{-1} \, s^{-1}}$. For the CFD analyses, the non-slide condition is applied at the solid–fluid interfaces. The inlet velocity is set as $50 \, \mathrm{\mu m \, s^{-1}}$ and zero static pressure condition is applied at the outlet boundaries to simulate the fluidic behaviors in porous structures, unless otherwise stated.

Results and Discussion

2D Cross-Sectional Designs for Fluid Channels

Uniform Fluid Velocity: Shape Optimization

The examples shown here aim to seek the optimal configurations of uniaxial fluidic channels for uniform distribution of WSS at the cross-sectional area (Fig. 2a). Figure 3 shows the optimization processes, starting from a curved cross channel (iteration step $m = 1$). As the fluidic domain (top row) and level-set function $\Phi(\mathbf{x})$ (bottom row)

Figure 2. Two different design cases: (a) quasi-3D micro-channel model and (b) full 3D model. [Color figure can be seen in the online version of this article, available at wileyonlinelibrary.com.]
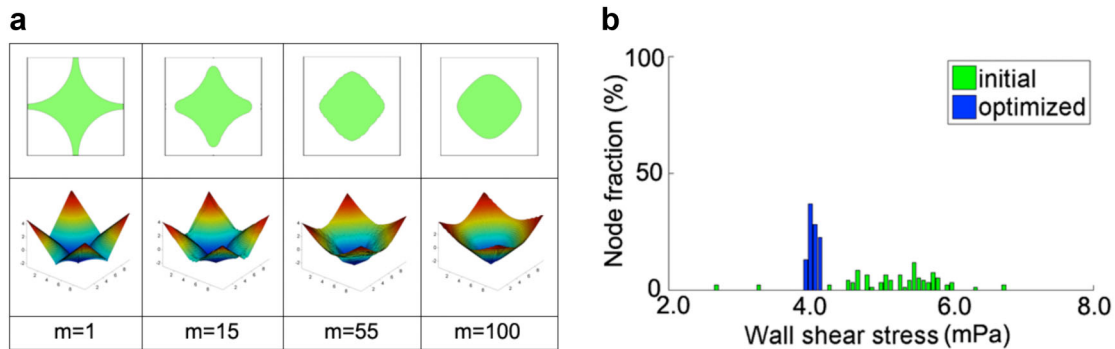
Figure 3. Case 1: design from a curved cross initial shape (100 mesh × 100 mesh). The porosity V_0 is 35%. **a**: Upper row: fluid domain; lower row: level-set function. m is the iteration number. **b**: Initial and optimized WSS distribution. [Color figure can be seen in the online version of this article, available at wileyonlinelibrary.com.]

evolve, the WSS criterion drives the configuration of fluid domain towards a circular shape, yielding a more uniform WSS distribution at the fluid–solid interface (Fig. 3b). It is observed that driven by the deviation between the local WSS and the mean value, the ends of the cross bars progressively shrink inwards while, in contrast, the central region dilates. Finally, the bar-ends vanish and gradually form a circle at the center of design domain.

Figure 4 shows a similar optimization process but starting from a rectangular initial shape. Once again, one can see that a centrally positioned circle is finally formed. To observe the WSS distributions, Figures 3b and 4b compare the WSS histograms in the initial and optimized fluid channels for these two cases, respectively. It can be clearly seen that the initial WSS (green) distribution was fairly spread out, while the final distributions (blue) become much more uniform.

Gradient Fluid Velocity: Topology Optimization

In the abovementioned two cases, a uniform inlet flow was presented at Γ_{in}, and finally the optimization takes a circular shape. For a uniform inlet flow, one may argue that multiple circular channels can also achieve the objective of a uniform WSS as defined in Equation (3). However, if the inlet flow presents in a fully developed laminar pattern in a given sectional area, for example, in a blood vessel or bioreactor chamber, such a multi-hole design may not be applicable. Under this circumstance, we assume that the inlet flow at Γ_{in} is prescribed in a theoretical solution to an incompressible laminar flow through a tube with a long rectangular cross-sectional guide, where the velocity at the domain center reaches its highest value, while the one at the boundary of design domain is reduced to zero.

To deal with such a flow case, we consider an initial design consisting of four symmetrical circles as shown in Figure 5. The design progresses in two ways: on one hand, the interface close to the center presents a higher WSS, leading to the fluid boundary propagating outwards; on the other hand, the fluid interface next to the boundaries has a lower WSS, resulting in an inward movement. As a result, these four initial circular fluidic channels tend to gradually move towards the center and finally form a bigger circle to minimize the WSS deviation in the domain.
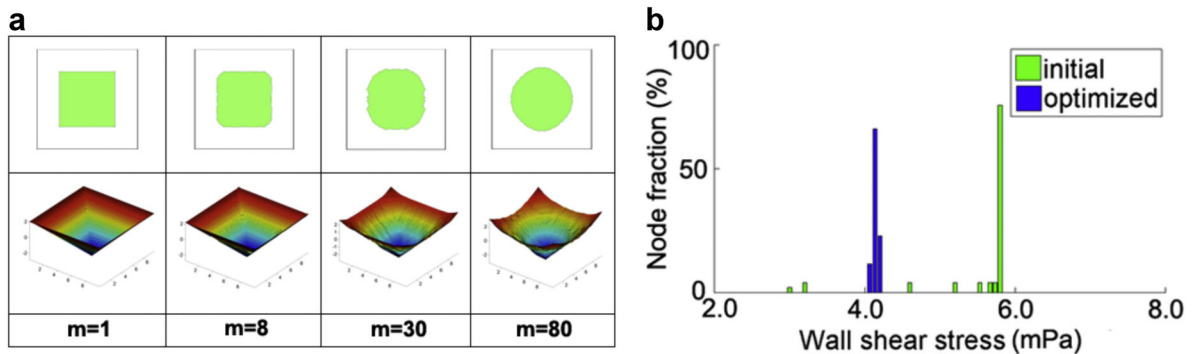
Figure 4. Case 2: design from a rectangular initial shape (100 mesh × 100 mesh). The porosity V_0 is 35%. **a**: Upper row: fluid domain; lower row: level-set function. m is the iteration number. **b**: Initial and optimized WSS distribution. [Color figure can be seen in the online version of this article, available at wileyonlinelibrary.com.]
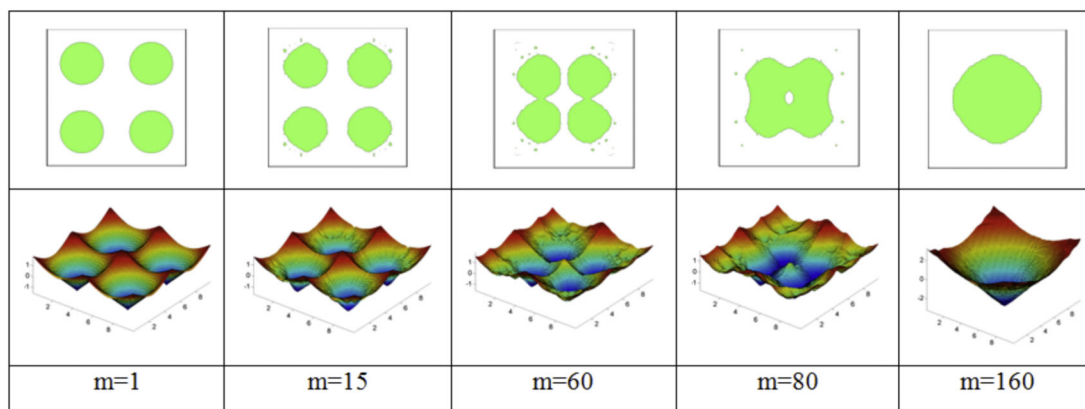
Figure 5. Case 3: design from multi-circles under a developed flow pattern generated by a long guide (100 mesh × 100 mesh). The non-uniform inflow leads to a unique optimal solution. The porosity V_0 is 35%. Upper row: fluid domain; lower row: level-set function. [Color figure can be seen in the online version of this article, available at wileyonlinelibrary.com.]

3D Designs for the Cellular Microstructure

To optimize the topology of a 3D base-cell, periodic boundary conditions are applied to both level-set function $\Phi(\mathbf{x})$ and CFD simulations at all the exterior faces of the base-cell domain. Two different cases, namely single- and tri-directional flows, are considered respectively.

Single-Directional Flow Design

In the first 3D case, only one pair of inlet and outlet is prescribed to the design domain as shown in Figure 2b, which indicates a single directional flow through the base-cell. The intermediate and optimal results are presented in Figure 6. In the optimization process, the radius of flow cylinder along the inlet–outlet direction increases, while the other four lateral guides gradually shrink and finally disappear. Thus, a single cylindrical fluidic channel with a larger diameter is created inside the cell unit. It can be observed that the distribution of WSS finally becomes much more uniform in the optimal base-cell topology. Thus, such a periodic scaffold has multiple parallel channels in the flow direction. As shown in the WSS histogram diagram, it is interesting to note that, as green elements gradually disappear, the high percentage of zero or very low level of WSS shifts to a more desirable mean level. Figure 7 provides the convergence history of the objective function (Eq. 3) as well as some evolving snapshots of resultant cellular structures.

Tri-Directional Flow Design With Bi-Connected Solid Domain

In this case, the optimal design of a tri-directional flow through porous material is presented. For the purpose of ensuring the effectiveness and stability of proposed level-set-based algorithm, an initial design with four parallel bars (i.e., a bi-connected structure) is adopted herein. From
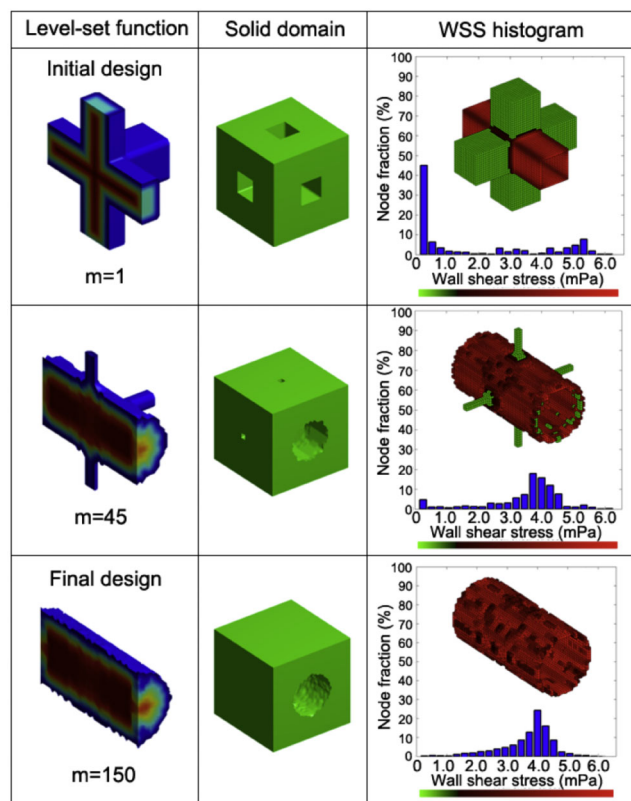
Figure 6. In 3D single-directional flow design, a mono-cylindrical fluid domain is obtained. The volume fraction V_0 is 40%. Fluidic domain is represented by the level-set function. WSS at interfaces is regulated to 0–1, as indicated by a color bar. The final design shows that the WSS distribution has become much more uniform. [Color figure can be seen in the online version of this article, available at wileyonlinelibrary.com.]
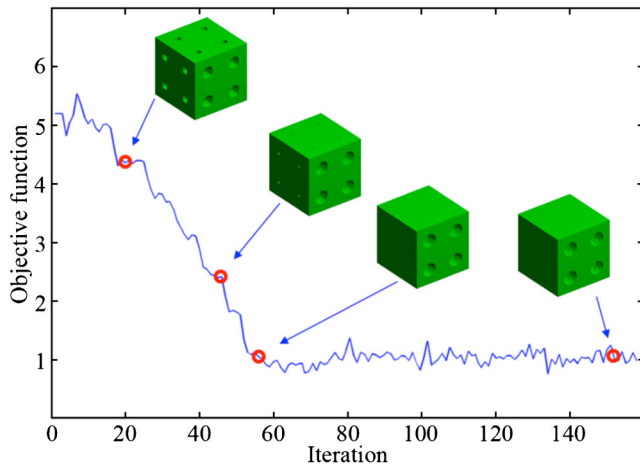
Figure 7. Convergence history of the objective function and corresponding cellular structures ($2 \times 2 \times 2$) for 3D single-directional flow design. [Color figure can be seen in the online version of this article, available at wileyonlinelibrary.com.]

Figure 8, it can be seen that a Schwarz-P like topology (Rajagopalan and Robb, 2006), a representative mosaic of minimal surfaces, gradually emerges. During the design process, the WSS distribution becomes more and more uniform, though the topology appears more complicated than that in the mono-directional flow case due to the sophistication required for accommodating tri-directional flow in the base-cell. Since the pairs of inlet and outlet regions are perpendicular and close to one another, the WSS reaches its maximum at the corners but lowest at the center of the design domain. Hence, based on the WSS criterion, a tri-continuous pore configuration has gradually taken shape and connected tri-directionally with adjacent base-cells through the periodic boundaries. From the resemblance to a Schwarz-P surface, it is suggested that a general constant mean curvature (CMC; Zhou and Li, 2007) interface can also lead to a uniformly distributed WSS in the optimized cellular structures. It is seen that although a certain degree of oscillation occurs at the early stage of optimization (Fig. 9), the objective function reaches its minimum after about 60 iterations.
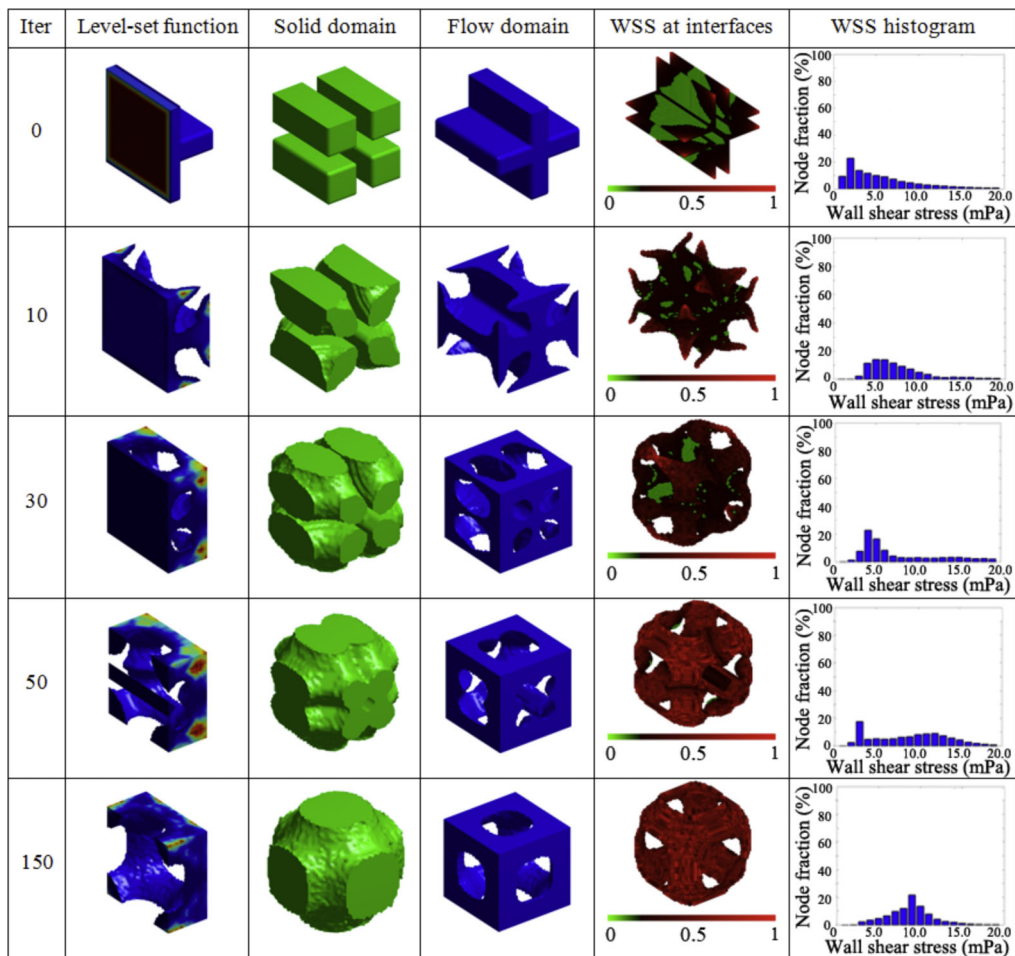
Figure 8. 3D Tri-directional flow design. The bi-connected solid domain starts to aggregate and finally forms a Schwarz-P-like structure in which its solid–fluid interface has a constant mean curvature, leading to a uniform WSS distribution. [Color figure can be seen in the online version of this article, available at wileyonlinelibrary.com.]
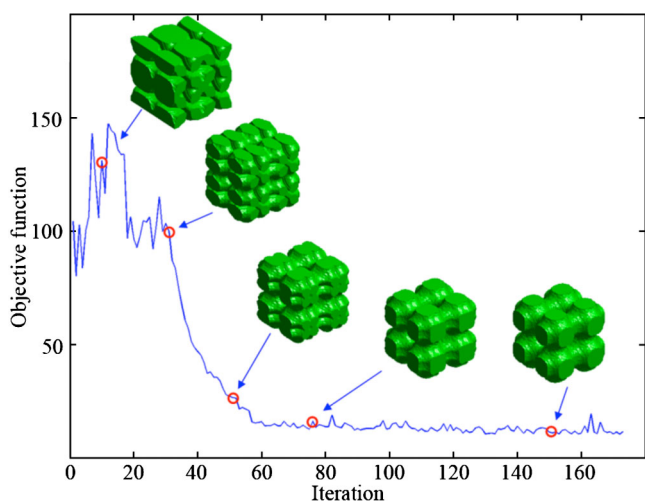
Figure 9. Convergence history of the objective function and corresponding cellular structures ($2 \times 2 \times 2$) for 3D tri-directional flow design. [Color figure can be seen in the online version of this article, available at wileyonlinelibrary.com.]

Solid Free-Form Fabrication (SFF) of Designed 3D Cellular Structures

The above computational designs generate specific topologies with considerable geometric sophistication, which may be very difficult to manufacture via random fabrication techniques. With the development of solid free-form fabrication (SFF) technology, rapid-prototyping of biomaterials with cellular structures has shown significant benefits to *in vivo* and *in vitro* studies (Hutmacher et al., 2004; Lin et al., 2004, 2007; Starly et al., 2006; Sun et al., 2004). To demonstrate how these designed cellular structures are fabricated, we prototyped two samples with $6 \times 6 \times 6$ assembly of base-cells as shown in Figure 10.

The computer-aided design (CAD) parts are created by, firstly extracting the zero-level contours (solid–fluid interfaces) from level-set functions; secondly constructing the solid-phase topologies of base-cells using 3D CAD software; and finally converting those models into STL (stereolithography) format with smoothed surface representation. To better observe the architectural details, the base-cell dimension in the both models is scaled up from $200 \, \mu m$ to 1.4 mm, though the latest SFF technology allows implementing an even higher resolution (Hollister, 2009; Hutmacher et al., 2004). It can be clearly seen that the fabricated models exhibit a good topological resemblance to those optimized base-cells, which are expected to generate a desired uniform WSS distribution.

Conclusions

After understanding the significance of WSS in cell responses and tissue growth, this study developed a level-
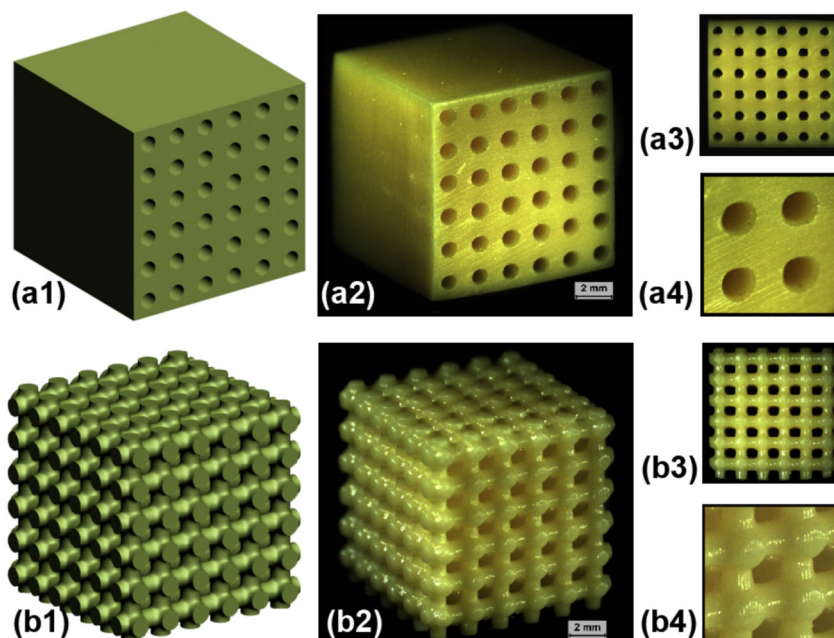
Figure 10. 3D cellular biomaterial designs for WSS criterion. The cellular material model is fabricated by the solid-free form fabrication (SFF) technology (Perfactory® III Standard, Envisiontec, Gladbeck, Germany), using SI-300 ABS simulant material. The printing resolution is 50 μm voxels in the *X, Y,* and *Z* dimensions. **a**1–**a**4: Single-directional flow design with cylindrical channels. **b**1–**b**4: Tri-directional flow design. Computational models (a1 and b1) are derived from the level-set functions of optimal designs, and smoothed for finer surface representation. Dimension of base-cells are scaled up from 200 μm to 1.4 mm in both cases, in order to reveal better architectural characteristics. [Color figure can be seen in the online version of this article, available at wileyonlinelibrary.com.]

set-based topology optimization approach to the design of porous biomaterials for a uniform WSS criterion. The main methodological features include: (1) the level-set function was used to trace boundary propagation in a smoother way compared with other density-based topology optimization methods; (2) the fluidic channels and porous base-cells were used to calculate the WSS at fluid interfaces; (3) the deviation between the local WSS and its target was adopted to drive the boundary movement in the level-set model; and (4) the CFD analysis was embedded in the level-set procedure. In this paper, designs of 2D cross-sectional (namely quasi-3D) and full 3D periodic base-cell were presented. In the quasi-3D examples, a microfluidic channel was extruded from the zero-level contour of a 3D level-set function. In the 3D design cases, mono- and tri-directional flows are considered in the different initial designs that were extracted from the 4D level-set functions. It is observed that in all these design cases, more uniform WSS distributions were achieved at the optimal fluidic interfaces. Interestingly, the optimized topologies of base-cells exhibited a CMC surface, regardless of the different predefined initial designs and flow conditions. From this perspective, the topological design appears critical in achieving desirable biomechanical features of cellular biomaterials. Following this design, SFF technique was exploited to prototype two such 3D WSS-based structures. In summary, the paper provides a means to developing a porous medium with a desired WSS pattern. It is expected that these uniform WSS designs can potentially enable cells to differentiate and tissue to grow in a more uniform and controllable way (Cioffi et al., 2006; Gutierrez and Crumpler, 2008; Williams et al., 2002). This study contributes a novel approach to the existing fluidic characterization techniques and successful scaffold design methods (Lin et al., 2005, 2007; Zhang et al., 2009). The proposed method exhibits considerable potential in developing novel cellular biomaterials for new prosthetic applications, for example, in tissue scaffold, vascular stent and porous coated implant.

References

Bendsoe MP, Sigmund O. 2003. Topology, optimization: Theory, methods, and applications Berlin. New York: Springer, p. 370.

Boschetti F, Raimondi MT, Migliavacca F, Dubini G. 2006. Prediction of the micro-fluid dynamic environment imposed to three-dimensional engineered cell systems in bioreactors. J Biomech 39(3):418–425.

Challis VJ, Guest JK. 2009. Level set topology optimization of fluids in stokes flow. Int J Numerical Methods Eng 79:1284–1308.

Chen YH, Zhou SW, Li Q. 2009. Computational design for multifunctional microstructural composites. Int J Mod Phys B 23(6–7):1345–1351.

Chung CA, Chen CW, Chen CP, Tseng CS. 2007. Enhancement of cell growth in tissue-engineering constructs under direct perfusion: Modeling and simulation. Biotechnol Bioeng 97(6):1603–1616.

Cioffi M, Boschetti F, Raimondi MT, Dubini G. 2006. Modeling evaluation of the fluid-dynamic microenvironment in tissue-engineered constructs: A micro-CT based model. Biotechnol Bioeng 93(3):500–510.

Davies PF. 1995. Flow-mediated endothelial mechanotransduction. Physiol Rev 75(3):519–560.

Gao H, Ayyaswamy PS, Ducheyne P. 1997. Dynamics of a microcarrier particle in the simulated microgravity environment of a rotating-wall vessel. Microgravity Sci Technol 10(3):154–165.

Gemmiti CV, Guldberg RE. 2009. Shear stress magnitude and duration modulates matrix composition and tensile mechanical properties in engineered cartilaginous tissue. Biotechnol Bioeng 104(4):809–820.

Gibson LJ. 2005. Biomechanics of cellular solids. J Biomech 38(3):377–399.

Guest JK, Prevost JH. 2006. Optimizing multifunctional materials: Design of microstructures for maximized stiffness and fluid permeability. Int J Solids Struct 43(22–23):7028–7047.

Guest JK, Prevost JH. 2007. Design of maximum permeability material structures. Comput Methods Appl Mech Eng 196(4–6):1006–1017.

Gutierrez RA, Crumpler ET. 2008. Potential effect of geometry on wall shear stress distribution across scaffold surfaces. Ann Biomed Eng 36(1):77–85.

Hassani B, Hinton E. 1998. A review of homogenization and topology optimization I—Homogenization theory for media with periodic structure. Comput Struct 69(6):707–717.

Hillsley MV, Frangos JA. 1994. Bone tissue engineering—The role of interstitial fluid-flow—Review. Biotechnol Bioeng 43(7):573–581.

Hollister SJ. 2005. Porous scaffold design for tissue engineering. Nat Mater 4(7):518–524.

Hollister SJ. 2009. Scaffold design and manufacturing: From concept to clinic. Adv Mater 21(32–33):3330–3342.

Hollister SJ, Lin CY. 2007. Computational design of tissue engineering scaffolds. Comput Methods Appl Mech Eng 196(31–32):2991–2998.

Hollister SJ, Maddox RD, Taboas JM. 2002. Optimal design and fabrication of scaffolds to mimic tissue properties and satisfy biological constraints. Biomaterials 23(20):4095–4103.

Hutmacher DW, Singh H. 2008. Computational fluid dynamics for improved bioreactor design and 3D culture. Trends Biotechnol 26(4):166–172.

Hutmacher DW, Sittinger M, Risbud MV. 2004. Scaffold-based tissue engineering: Rationale for computer-aided design and solid free-form fabrication systems. Trends Biotechnol 22(7):354–362.

Johnson DL, McAllister TN, Frangos JA. 1996. Fluid flow stimulates rapid and continuous release of nitric oxide in osteoblasts. Am J Physiol Endocrinol Metab 271(1):E205–E208.

Kang H, Lin CY, Hollister SJ. 2010. Topology optimization of three dimensional tissue engineering scaffold architectures for prescribed bulk modulus and diffusivity. Struct Multidiscip Optimization. 10.1007/s00158-010-0508-8.

Katayama T, Yamamoto H, Takimoto K. 1999. Solid–fluid biomimetic composites by considering load dispersion mechanism of cancellous bone structure (consideration of honeycomb structure). JSME Int J Ser A-Solid Mech Mater Eng 42(3):355–361.

Klein-Nulend J, Bacabac RG, Mullender MG. 2005. Mechanobiology of bone tissue. Pathol Biol 53(10):576–580.

Lacroix D, Planell JA, Prendergast PJ. 2009. Computer-aided design and finite-element modelling of biomaterial scaffolds for bone tissue engineering. Philos Trans R Soc A-Math Phys Eng Sci 367(1895):1993–2009.

Lesman A, Blinder Y, Levenberg S. 2010. Modeling of flow-induced shear stress applied on 3d cellular scaffolds: Implications for vascular tissue engineering. Biotechnol Bioeng 105(3):645–654.

Lin CY, Hsiao CC, Chen PQ, Hollister SJ. 2004. Interbody fusion cage design using integrated global layout and local microstructure topology optimization. Spine 29(16):1747–1754.

Lin CY, Schek RM, Mistry AS, Shi XF, Mikos AG, Krebsbach PH, Hollister SJ. 2005. Functional bone engineering using ex vivo gene therapy and topology-optimized, biodegradable polymer composite scaffolds. Tissue Eng 11(9–10):1589–1598.

Lin CY, Wirtz T, LaMarca F, Hollister SJ. 2007. Structural and mechanical evaluations of a topology optimized titanium interbody fusion cage fabricated by selective laser melting process. J Biomed Mater Res A 83(2):272–279.

Maes F, Ransbeeck P, Van Oosterwyck H, Verdonck P. 2009. Modeling fluid flow through irregular scaffolds for perfusion bioreactors. Biotechnol Bioeng 103(3):621–630.

McAllister TN, Frangos JA. 1999. Steady and transient fluid shear stress stimulate NO release in osteoblasts through distinct biochemical pathways. J Bone Miner Res 14(6):930–936.

Meinel L, Karageorgiou V, Fajardo R, Snyder B, Shinde-Patil V, Zichner L, Kaplan D, Langer R, Vunjak-Novakovic G. 2004. Bone tissue engineering using human mesenchymal stem cells: Effects of scaffold material and medium flow. Ann Biomed Eng 32(1):112–122.

Milan JL, Planell JA, Lacroix D. 2009. Computational modelling of the mechanical environment of osteogenesis within a polylactic acid–calcium phosphate glass scaffold. Biomaterials 30(25):4219–4226.

Osher S, Sethian JA. 1988. Fronts propagating with curvature-dependent speed—Algorithms based on Hamilton–Jacobi formulations. J Comput Phys 79(1):12–49.

Porter B, Zauel R, Stockman H, Guldberg R, Fyhrie D. 2005. 3-D computational modeling of media flow through scaffolds in a perfusion bioreactor. J Biomech 38(3):543–549.

Powers MJ, Rodriguez RE, Griffith LG. 1997. Cell-substratum adhesion strength as a determinant of hepatocyte aggregate morphology. Biotechnol Bioeng 53(4):415–426.

Provin C, Takano K, Sakai Y, Fujii T, Shirakashi R. 2008. A method for the design of 3D scaffolds for high-density cell attachment and determination of optimum perfusion culture conditions. J Biomech 41(7):1436–1449.

Rajagopalan S, Robb RA. 2006. Schwarz meets Schwann: Design and fabrication of biomorphic and durataxic tissue engineering scaffolds. Med Image Anal 10:693–712.

Rose F, Oreffo ROC. 2002. Bone tissue engineering: Hope vs hype. Biochem Biophys Res Commun 292(1):1–7.

Saini S, Wick TM. 2001. Modulation of Biochemical Properties of Engineered Cartilage Constructs; ASME BED-2001, Bioengineering Conference, p. 185–186.

Sakai K, Mohtai M, Iwamoto Y. 1998. Fluid shear stress increases transforming growth factor beta 1 expression in human osteoblast-like cells: Modulation by cation channel blockades. Calcif Tissue Int 63(6):515–520.

Sethian JA, Wiegmann A. 2000. Structural boundary design via level set and immersed interface methods. J Comput Phys 163(2):489–528.

Smalt R, Mitchell FT, Howard RL, Chambers TJ. 1997. Induction of NO and prostaglandin E-2 in osteoblasts by wall-shear stress but not mechanical strain. Am J Physiol Endocrinol Metab 273(4):E751–E758.

Starly B, Lau W, Bradbury T, Sun W. 2006. Internal architecture design and freeform fabrication of tissue replacement structures. Comput Aided Des 38(2):115–124.

Steven GP, Li Q, Xie YM. 2000. Evolutionary topology and shape design for general physical field problems. Comput Mech 26(2):129–139.

Sun W, Starly B, Darling A, Gomez C. 2004. Computer-aided tissue engineering: Application to biomimetic modelling and design of tissue scaffolds. Biotechnol Appl Biochem 39:49–58.

Wang MY, Wang XM, Guo DM. 2003. A level set method for structural topology optimization. Comput Methods Appl Mech Eng 192(1–2):227–246.

Williams KA, Saini S, Wick TM. 2002. Computational fluid dynamics modeling of steady-state momentum and mass transport in a bioreactor for cartilage tissue engineering. Biotechnol Progr 18(5):951–963.

Zhang HN, Lin CY, Hollister SJ. 2009. The interaction between bone marrow stromal cells and RGD-modified three-dimensional porous polycaprolactone scaffolds. Biomaterials 30(25):4063–4069.

Zhou SW, Li Q. 2007. The relation of constant mean curvature surfaces to multiphase composites with extremal thermal conductivity. J Phys D Appl Phys 40:6083–6093.

Zhou SW, Li Q. 2008. A variational level set method for the topology optimization of steady-state Navier–Stokes flow. J Comput Phys 227(24):10178–10195.